JACC: BASIC TO TRANSLATIONAL SCIENCE VOL. 5, NO. 3, 2020

PRECLINICAL RESEARCH

Dynamic Augmentation of Left Ventricle and Mitral Valve Function With an Implantable Soft Robotic Device

Mossab Y. Saeed, MD,[a] David Van Story, BE,[a] Christopher J. Payne, PhD,[a,b,c] Isaac Wamala, MD,[a] Borami Shin, MD,[a] Daniel Bautista-Salinas, MSc,[a,d] David Zurakowski, PhD,[e] Pedro J. del Nido, MD,[a] Conor J. Walsh, PhD,[b,c] Nikolay V. Vasilyev, MD[a]

VISUAL ABSTRACT

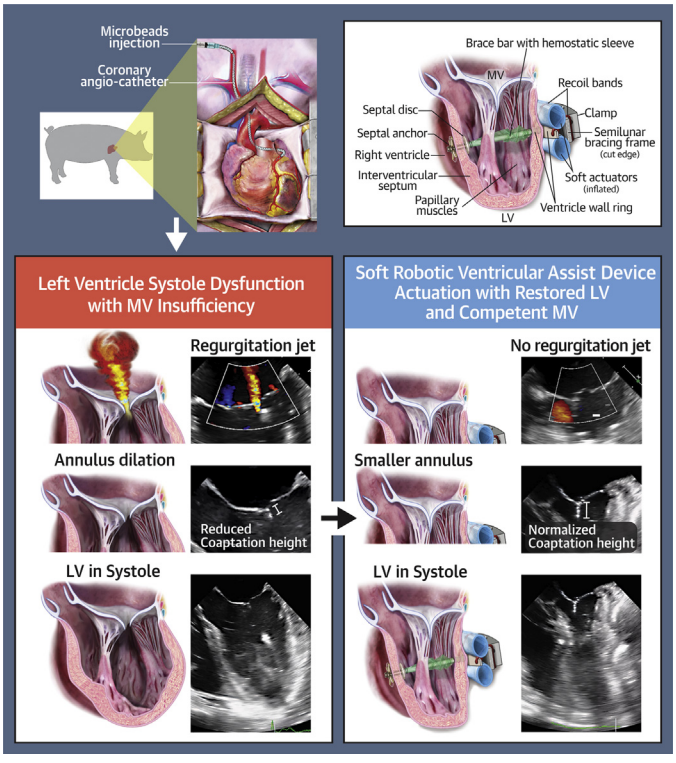

Saeed, M.Y. et al. J Am Coll Cardiol Basic Trans Science. 2020;5(3):229-42.

HIGHLIGHTS

- **LVSD is associated with reduced LV systolic function and geometrical changes.**
- **MVR results from LVSD.**
- **Current management strategies address LVSD and secondary MVR separately, even in advanced stages of LVSD.**
- **We describe an implantable soft robotic device that would provide a new paradigm in supporting patients with coexistence of LVSD and concomitant MVR by dynamically augmenting native LV contraction and supporting the mitral valve apparatus to eliminate the associated MVR.**

ISSN 2452-302X https://doi.org/10.1016/j.jacbts.2019.12.001

JACC: BASIC TO TRANSLATIONAL SCIENCE VOL. 5, NO. 3, 2020
MARCH 2020:229–42

ABBREVIATIONS AND ACRONYMS

FS = fractional shortening

HF = heart failure

IQR = interquartile range

IVS = interventricular septum

LHF = left heart failure

LV = left ventricular

LVEDP = left ventricular end-diastolic pressure

LVSD = left ventricular systolic dysfunction

MV = mitral valve

MVR = mitral valve regurgitation

RV = right ventricle

SRVAD = soft robotic ventricular assist device

SUMMARY

Left ventricular failure is strongly associated with secondary mitral valve regurgitation. Implantable soft robotic devices are an emerging technology that enables augmentation of a native function of a target tissue. We demonstrate the ability of a novel soft robotic ventricular assist device to dynamically augment left ventricular contraction, provide native pulsatile flow, simultaneously reshape the mitral valve apparatus, and eliminate the associated regurgitation in an Short-term large animal model of acute left ventricular systolic dysfunction. (J Am Coll Cardiol Basic Trans Science 2020;5:229–42) © 2020 The Authors. Published by Elsevier on behalf of the American College of Cardiology Foundation. This is an open access article under the CC BY-NC-ND license (http://creativecommons.org/licenses/by-nc-nd/4.0/).

Heart failure (HF) represents a significant health care burden, affecting 5.7 million patients in the United States, with an estimated annual incidence of 20%, and the prevalence is expected to increase by 46% by 2030. The national HF costs reached $39.83 billion in 2014, with projections suggesting that by 2030, the total cost of HF will increase to $69.7 billion (1–3). Current guidelines subdivide left heart failure (LHF) into LHF with preserved ejection fraction, also known as diastolic LHF, and LHF with reduced ejection fraction, also known as systolic LHF (4). Different strategies have been developed in clinical practice to treat different types of LHF, depending on the underlying cause, impact on quality of life, and stage of the disease (1,2). Most of the strategies start with lifestyle changes and medication in stages A and B, moving to surgical intervention in stage C, and then to ventricular assist devices in stage D as a destination therapy or as a bridge for transplantation, with a limited window of hope for ventricular recovery (5).

LHF with reduced ejection fraction is defined as left ventricular systolic dysfunction (LVSD) with an ejection fraction of <40%. The prevalence of LHF with reduced ejection fraction is 6% in symptomatic patients, 5% in asymptomatic patients, and about 3% in the general population. LVSD is associated with an increased incidence of symptomatic HF and mortality (3,6,7).

SEE PAGE 243

In patients with LHF, the shape and function of the LV chamber and the mitral valve (MV) apparatus are closely interrelated (8,9). In the majority of patients, the MV is structurally normal, while LV dilatation and an increase in the distance between the LV free wall and interventricular septum (IVS) leads to papillary muscles dislocation, chordae tethering, and loss of leaflet coaptation, which leads to development of secondary MV regurgitation (MVR). Furthermore, LV dilatation leads to MV annulus dilatation and flattening, which contributes to loss of leaflet coaptation height and worsens progression of the LHF (10,11). MVR is present in up to 56.2% (mild in 39.4% and moderate to severe in 16.8%) of patients with LVSD. The coexistence of 2 conditions make the care of this subset of patients more challenging and increase their mortality risk (10,12,13).

Current management strategies address the LHF and secondary MVR separately, even in advanced stages of the LHF (4,5,14).

From the [a]Department of Cardiac Surgery, Boston Children's Hospital, Harvard Medical School, Boston, Massachusetts; [b]Wyss Institute for Biologically Inspired Engineering, Harvard University, Boston, Massachusetts; [c]John A. Paulson Harvard School of Engineering and Applied Sciences, Harvard University, Boston, Massachusetts; [d]School of Industrial Engineering, Technical University of Cartagena, Cartagena, Spain; and the [e]Department of Anesthesiology, Critical Care and Pain Medicine, Boston Children's Hospital, Harvard Medical School, Boston, Massachusetts. This work was supported in part by the U.S. Department of Defense Congressionally Directed Medical Research Programs Discovery Award W81XWH-15-1-0248 (to Dr. Vasilyev), the Wyss Institute for Biologically Inspired Engineering, and the Harvard John A. Paulson School of Engineering and Applied Sciences. Drs. Payne and Vasilyev were the inventors and are listed on a patent application related to the research presented in this paper submitted on June 24, 2016, application number 62/354,196. Dr. Vasilyev is currently an employee of Pfizer. All other authors have reported that they have no relationships relevant to the contents of this paper to disclose.
The authors attest they are in compliance with human studies committees and animal welfare regulations of the authors' institutions and Food and Drug Administration guidelines, including patient consent where appropriate. For more information, visit the *JACC: Basic to Translational Science* author instructions page.

Manuscript received August 20, 2019; revised manuscript received December 3, 2019, accepted December 3, 2019.

Several beating-heart surgical and transcatheter device therapies have been developed, with the aim of statically restraining either the MV annulus and leaflets or the LV chamber and subvalvar components of the MV (15). Fundamentally, currently available surgical and transcatheter therapies for secondary MVR are limited in that they rely on passive, often nonphysiologic restraint of the MV and LV structures, while MVR is dynamic in nature (16). The MitraClip (Abbott Laboratories, Abbott Park, Illinois) is a percutaneous mechanical device that performs an edge-to-edge approximation of the MV leaflets similar to the surgical technique developed by Maisano et al. (17). With 96% procedural success rate and reducing MR and LV volume overload, the MitraClip showed 3.2% early technical failure and 24.8% need reoperation for recurrent MVR, while 45% of patients had grade 3+ to 4+ MR at 1-year follow-up (18,19). Several catheter-based devices have been developed for indirect (via coronary sinus) and direct MV annuloplasty. The Carillon Mitral Contour System device (Cardiac Dimensions, Kirkland, Washington) was evaluated clinically, but in the latest (TITAN II [Transcatheter Implantation of Carillon Mitral Annuloplasty Device II]) trial, 25% of patients had grade 3+ to 4+ MR at 1-year follow-up, with one-third reporting HF-related hospitalizations (20). The Coapsys device (Myocor, Maple Grove, Minnesota) was an innovative concept for LV remodeling that aimed to reduce LV free wall to IVS distance at the papillary muscle level. Despite early termination of the RESTOR-MV (Randomized Evaluation of a Surgical Treatment for Off-Pump Repair of the Mitral Valve) trial for financial reasons, initial results indicated a lack of benefit of Coapsys implantation when used in combination with coronary artery bypass grafting surgery, with lower MR grades measured in the control group after 2 years ($p < 0.001$) (21).

For LV augmentation, ventricular assist devices are a well-established technology utilized in late stages of LHF. The ventricular assist device is typically connected between the LV, where the inflow cannula is placed via an invasive surgical approach or delivered percutaneously via peripheral vessel, and the aorta. Therefore, ventricular assist devices take over LV function by rerouting blood flow from the failed LV but provide no solution for the MVR. Design of currently available ventricular assist devices is based on the principle of continuous blood flow through an artificial lumen of the device. Lack of pulsatility results in the loss of high-molecular-weight multimer of von Willebrand factor, which leads to serious complications such as gastrointestinal bleeding in up 30% of patients (22).

We have previously developed a soft robotic Ventricular assist device (SRVAD) with septal bracing (**Figure 1**) that synchronously approximates the ventricular free wall and the IVS with native ventricular contraction and provides dynamic support to ventricular systolic function (23). In a prior study, we showed that timing and synchronization is important for effective augmentation of the ventricular blood volume ejection (23). In this study, we aimed to support our preliminary results and investigate the device's ability to augment the LV geometry, restore the LV systolic function, and simultaneously reshape the MV, eliminating the secondary MVR.

METHODS

EXPERIMENTAL DESIGN. The experimental protocol was approved by the Boston Children's Hospital Institutional Animal Care and Use Committee. All animals received humane care under the 1996 Guide for the Care and Use of Laboratory Animals recommended by the U.S. National Institutes of Health.

After establishing general anesthesia and ventilation in adult size Yorkshire pig (Parsons EM and Sons, Hadley, Massachusetts), we accessed the LV through a left-side thoracotomy incision. After placing monitoring instrumentation, we induced acute LVSD and then deployed the SRVAD in the same way for all animals. Device actuation supported the LV for 30 min. By the end of the experiment, we euthanized all animals by using Fatal-Plus Solution (Vortech Pharmaceuticals, Dearborn, Michigan) at a dose of 110 mg/kg/body weight. All hemodynamic data and echocardiographic functional data were acquired throughout the procedure at a healthy baseline, after induction of LVSD, and during device actuation.

IMPLANTABLE SRVAD WITH SEPTAL BRACING. The SRVAD (**Figure 1**) is a composite of soft actuators and a bracing system that applies synchronized cyclic loading to the LV free wall, with the forces transmitted to the IVS (23). The bracing assembly consists of a septal anchor that "sandwiches" the IVS between the septal anchor and disc, a bracing bar with a sealing sleeve that passes through the LV free wall, and a curved bracing frame that surrounds the ventricle in a parallel plane to the atrioventricular groove, and is limited by the anterior and posterior descending coronary arteries. The curved bracing frame incorporates embedded soft actuators that are based on the McKibben pneumatic artificial muscle design, providing external compression to the outer ventricle wall. The actuators are constrained in a curved configuration within the frame so that they straighten and radially expand when actuated. The actuators are

FIGURE 1 Soft Robotic Ventricular Assist Device With Septal Bracing

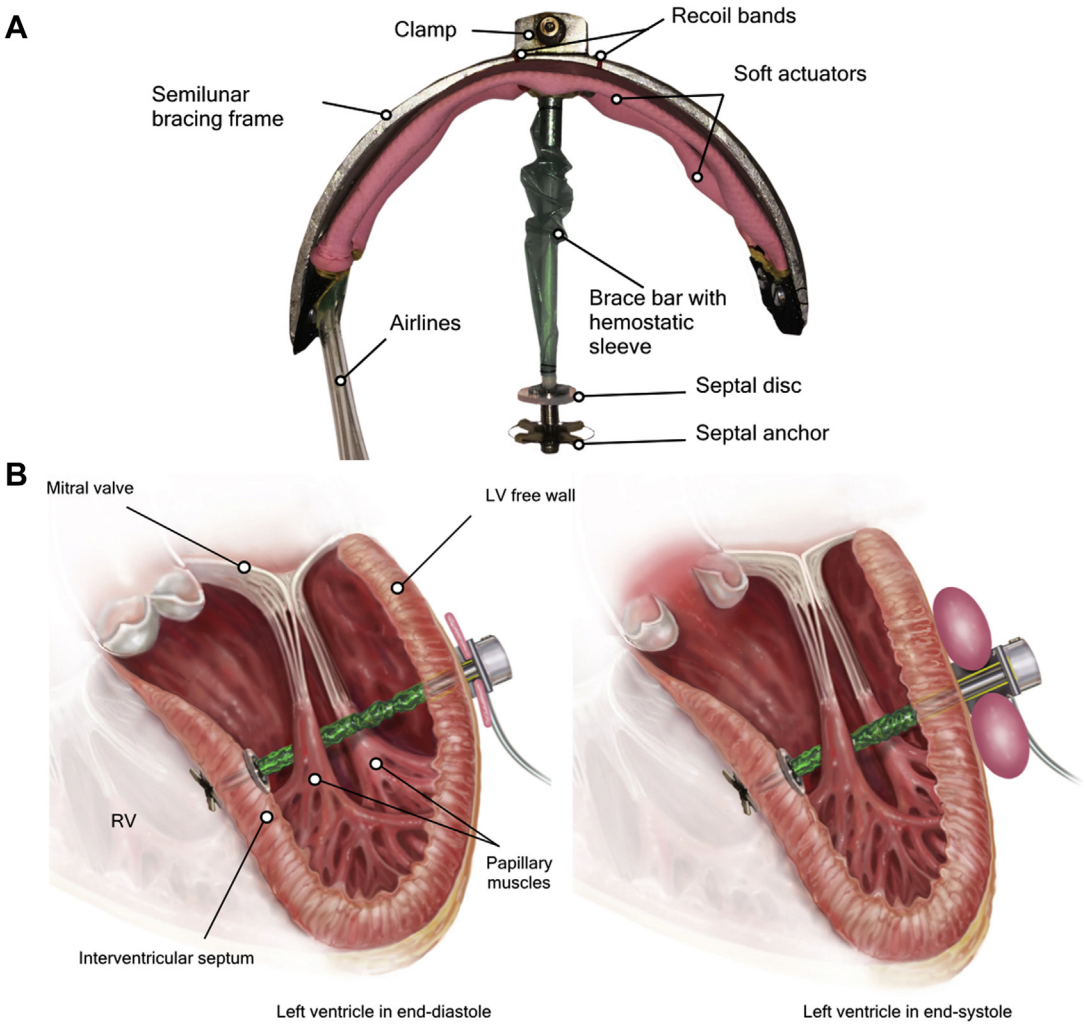

(A) Annotated photograph of the device used for left ventricular (LV) support. **(B)** Optimum device position from the LV free wall to the interventricular septum and the geometric differences between end-diastole **(left)** and end-systole **(right)** of the LV cavity and mitral valve annulus and coaptation height with device actuation. RV = right ventricle.

attached only to the bracing frame but not to the ventricular free wall. During the diastolic phase of the cardiac cycle, the actuators completely recoil back to the curved configuration within the frame.

ANESTHESIA AND SURGICAL INSTRUMENTATION. Pigs were initially sedated with Telazol (2.2 to 4.4 mg/kg) and xylazine (1 to 2 mg/kg) through intramuscular injection. General anesthesia was then established with isoflurane (3% induction) followed by endotracheal intubation. A Veterinary Anesthesia Ventilator (Model 2000, Hallowell EMC, Pittsfield, Massachusetts) was used to maintain frequency and deliver a maintenance anesthetic dose of isoflurane (0.5% to 2.0%) throughout the study. Ventilatory frequency and volume were adjusted to maintain arterial blood gas values within the physiological range (pH 7.35 to 7.45, partial pressure of carbon dioxide 30 to 40 mm Hg, partial pressure of oxygen 85 to 100 mm Hg). Core temperature was maintained at >36°C. Central venous access was established via the femoral vein, and continuous arterial blood pressure was monitored via carotid arterial catheters. During the experiments, lidocaine infusion (5 to 50 μg/kg/min) was administered to minimize the risk of ventricular arrhythmias. After placing the animal in the left lateral position, we

performed a left lateral thoracotomy incision and entered the pleural space through the fourth or fifth intercostal space. After opening the pericardium, we used 2/0 silk sutures as stay sutures to enhance exposure. To register the hemodynamic data, we placed flow probes (16PS and 20PS, Transonic Corporation, Ithaca, New York) on the aorta and pulmonary artery. A 5-F umbilical catheter connected to pressure transducers (SurgiVet, Smiths Medical, Minneapolis, Minnesota) was placed in the ascending aorta and left atrium. An additional 7-F VSL conductance pressure catheter (Transonic Corporation) was placed inside the LV. The pressure transducer and electrocardiography signals were transmitted to a clinical monitoring system (SurgiVet, Smiths Medical, Minneapolis, Minnesota). In addition to the device control system, a signal indicated the instantaneous state of the actuator control valve; all signals were then acquired in real time by a data logging system (Power Lab; model PL3516, ADInstruments, Dunedin, New Zealand) and monitored on a computer with compatible software (LabChart, ADInstruments).

ACUTE LVSD MODEL. To induce acute LVSD, we used a well-established model of acute ischemia by injection of intracoronary polystyrene microspheres into the left coronary arterial system (Polysciences, Warrington, Pennsylvania) (24–26). First, we established arterial access with a longitudinal cutdown incision on the right side of the pig neck. After careful dissection, we exposed the right common carotid artery and introduced a 7-F arterial sheath. Under fluoroscopy guidance (XRE corporation angiography station, XRE Corp., Littleton, Massachusetts), we introduced a 5-F angiography catheter (Merit Medical Systems, South Jordan, Utah) through the arterial sheath and floated it to the left coronary ostium. Ten milliliters of iodine contrast solution (74% Ioversol, Optiray 350, Mallinckrodt, St. Louis, Missouri) was injected into the left coronary ostium over 5 s to visualize and establish the baseline anatomy of the coronary arteries. To create the LVSD model, we embolized small- and medium-sized coronary vessels by injection of polystyrene microspheres (50-μm diameter in a concentration of between 16×10^3 and 36×10^3; 100-μm diameter in a concentration of between 4×10^3 and 12×10^3) diluted in 10 ml of normal saline into the left main coronary artery over 10 s, with 5 to 10 min between injections. Most of the time, 2 injections of each size were adequate to induce significant HF. We added an extra injection or made a selective injection into the left anterior descending and circumflex coronary arteries in the case of a short left main artery. We also varied the concentration, depending on the animal's response to the first injection. After 30 to 60 min, we documented the LVSD with the hemodynamic data and echocardiography images.

DEVICE DEPLOYMENT STEPS. To deploy the device, we administered heparin (150 to 300 U/kg), aiming for an activated clotting time of more than 250 s, maintained throughout the procedure. All steps were done under epicardial echocardiography guidance with 2-dimensional and live 3-dimensional imaging modalities.

Using echocardiography, we identified an entry point midway between 2 papillary muscles on the LV free wall and midlevel between the papillary muscle head and the base. We aimed for a mid-septal position on the left side of the IVS and below the moderator band and septal papillary muscle on the right side of the IVS. We secured the entry point with a circular Teflon pledget (United States Plastic Corporation, Lima, Ohio) and 2 purse strings by using a 3/0 polypropylene suture and snared it with tourniquets.

Under echocardiography guidance, we passed a 5-F curved puncture needle from the entry point on the LV free wall through the LV cavity and the IVS, until it appeared inside the right ventricle (**Figure 2A**). That was followed by insertion of a guidewire and removal of the needle (**Figure 2B**). Three sequential dilators (12-F, 16-F, and 20-F) were used to enlarge the access (**Figure 2C**). A 20-F delivery sheath was introduced from the entry point and advanced through the IVS into the right ventricle (**Figure 2D**). A right-side foldable anchor was introduced through the delivery sheath and opened inside the right ventricle (**Figures 2E and 2F**). The delivery sheath was removed, and the open anchor was pulled back against the IVS. We dilated the entry point with a 30-F dilator to introduce a left-side disc, which "sandwiched" the IVS, and screwed it with the right-side anchor (**Figure 2G**). At this point, the anchor holder was removed and the brace bar with the cover sleeve introduced through the sheath, was fixed to the left-side disc (**Figure 2H**) and passed through the LV free wall (**Figure 2I**). The entry point was controlled by tightening the purse strings around the cover sleeve and the brace to prevent any bleeding and allow the LV free wall to move freely around the brace. Finally, we fastened the frame with the attached actuators (**Figure 1**) to the bar and connected the actuators to the control system.

CONTROL SYSTEM AND DEVICE ACTIVATION. A computer control system was used to operate the SRVAD by inflating and deflating the pneumatic

actuators in synchrony with the native heart. Details of the control system are described in Payne et al. (23). A pneumatic air supply and vacuum source and provided to a control box containing the computer system and pneumatic hardware. An electrically controlled pressure regulator (ITV series, SMC Corporation, Tokyo, Japan) was used to maintain air pressure supplied to the actuators. Electronically triggered pneumatic valving system (NVKF333-5G-01T, SMC Corporation) was used to precisely direct pressurized air and vacuum to the actuators to allow inflation and deflation. Triggering of the valve system was provided through a pressure-sensing catheter (Transonic Corporation) that was placed inside the LV. The pressure signal was acquired by the computer control system (cRIO-9030; National Instruments, Austin, Texas) that could detect the beginning of systole based on the very initial pressure increase due to the native systolic contraction. The computer control system could then accurately time the pressurization and vacuum phases to synchronize with the native heart, based on this input signal. The computer control system could also calculate the native heart rate and autonomously regulate the systolic-diastolic ratio to be 35% of the cardiac cycle period (23).

ECHOCARDIOGRAPHY IMAGE ACQUISITION AND ANALYSIS. In addition to monitoring device implantation, we acquired epicardial 2- and 3-dimensional echocardiographic images to assess LV and MV functions. For image acquisition, we used a Philips ie33 machine (Philips Ultrasound, Bothell, Washington) with X7-2 and X7-2t transducers. We acquired the images at normal baseline heart function, after induction of LVSD, and at 5 and 30 min of device actuation. All image analysis was done with QLAB software, version 10.5 (Philips Healthcare).

STATISTICAL ANALYSIS. We characterized the cardiac output resulting from the device over an extended period of operation. We considered consecutive cardiac cycles for the normal baseline, LVSD, and after 5 and 30 min from the start of device actuation. We used 10 consecutive cycles for analysis. We registered individual LV pressures (maximum), mean left atrial pressure, mean arterial pressure, and volume ejections from the pulmonary artery and aorta, in addition to LV end-diastolic pressure (LVEDP) and stroke volume. Normality was assessed with the Kolmogorov-Smirnov test on all continuous variables.

Descriptive statistics are reported as mean ± SD for normally distributed data and median and interquartile range (IQR) for skewed data. For statistical testing, a 1-way analysis of variance was used for hemodynamic data, with Bonferroni's multiple comparisons test for normally distributed data and Freidman's test with Dunn's multiple comparisons test for non-normally distributed data. For echocardiography data, we used the Wilcoxon matched-pairs signed rank test. We considered 2-sided $p < 0.05$ to be statistically significant. All analyses and graphs were performed by using Prism 8 software, version 8.0.1 (GraphPad Software, San Diego, California).

RESULTS

The SRVAD operation resulted in geometric changes of the LV chamber and MV apparatus, which translated into functional improvement of LV and MV. This dynamic support of SRVSD also restored pulsatile blood flow in physiological manner.

We used 7 Yorkshire pigs with an average weight of 79.5 ± 3.8 kg. The first animal was used to establish a short-term model of LVSD with MVR. We induced acute ischemic LVSD, implanted the SRVAD (Figure 1A) in the other 6 animals, and evaluated device function for over 30 min.

DEVICE OPERATION. The SRVAD worked in synchrony with native LV contraction, leading to geometric changes in the LV by approximating LV free wall movement toward the IVS during LV systole and moving away from the LV free wall during diastole, allowing adequate LV filling (Figure 1B). To determine the efficiency of the mechanical effect of the device, we acquired echocardiographic images and determined LV fractional shortening (FS) at 3 levels: basal, mid-LV, and apical (Figure 3D). Measured at the LV basal level, the device was able to restore FS from a mean of 15.50 ± 6.30% after induction of LVSD to 30.90 ± 7.90% ($p = 0.031$) that was similar to the baseline level (24.40 ± 4.20%; $p = 0.156$) (Figure 3A). At the mid-LV level, the FS improved from a mean of 22.40 ± 3.50% at LVSD to 45.80 ± 15.70% during device support ($p = 0.063$), which is similar to the baseline FS of 33.41 ± 10.80%; ($p = 0.063$) (Figure 3B). FS at the apical level showed the same trend, 42.50 ± 14.70% at baseline, 28.30 ± 13.40% at LVSD and 47.20 ± 17.30% at SRVAD operation, although it was not statistically significant ($p = 0.156$ between LVSD and device actuation and 0.843 between baseline and device actuation) (Figure 3C).

IMPROVEMENT OF MV FUNCTION. From echocardiography images, we evaluated the effect of dynamic approximation of the LV free wall toward the IVS during systole at the LV basal and at the level of papillary muscle heads. The anterior-posterior distance of the MV annulus delta between diastole and systole during device actuation was at mean of 1.07 ± 0.10 cm in comparison with 0.84 ± 0.10 cm

FIGURE 2 **Deployment of Intracardiac Component of Soft Robotic LV Assist Device With Septal Bracing Under Echocardiographic Guidance**

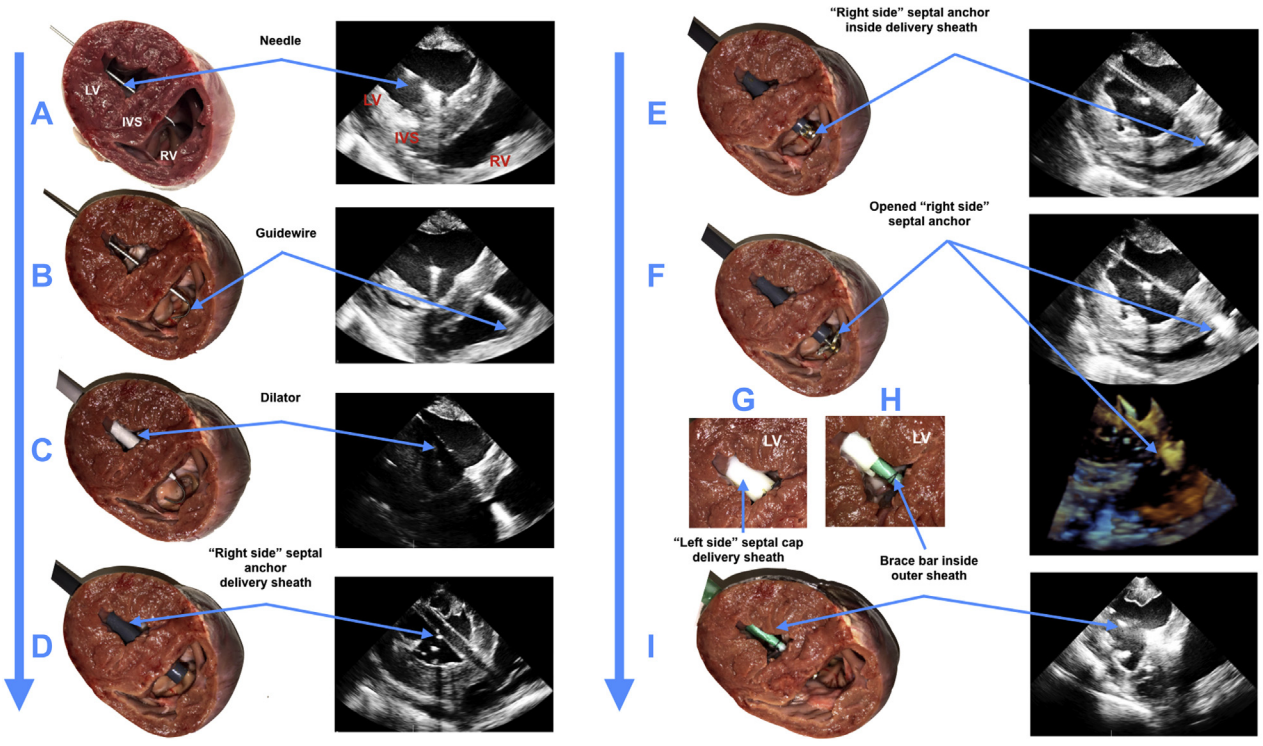

Ex vivo demonstrations are shown in the **left columns** and in vivo 2- and 3-dimensional echocardiography images are shown in the **right columns**. **(A)** Insertion of needle. **(B)** Introduction of the guidewire. **(C)** Dilator passed over the guidewire. **(D)** Insertion of a 20-F introducer sheath. **(E)** Deployment of a collapsible septal anchor. **(F)** Removal of the introducer sheath and retraction of the deployed septal anchor. **(G)** Introduction of a delivery tube and coupling of a tip-mounted septal disc on the right-side to left-side septal anchor. **(H)** Coupling of a bracing bar to the right-side septal disc and removal of the delivery tube. **(I)** Implanted brace with the covering sleeve shown in **green**. IVS = interventricular septum; LV = left ventricle; RV = right ventricle.

during the LVSD condition ($p = 0.031$) (Figure 4A). The changes in the MV annulus increased coaptation height from mean of 0.33 ± 0.20 cm during LVSD to 0.50 ± 0.20 cm ($p = 0.031$) during device actuation (Figure 4B). The device completely eliminated MVR and reduced the diameter of the vena contracta from mean of 0.35 ± 0.90 cm after the induction of LVSD to zero during the device actuation ($p = 0.125$) (Figure 5, Video 1).

AUGMENTATION OF LV FUNCTION. The resulting LV geometric changes at 5 min of cyclic device actuation from LVSD condition significantly increased the median LV maximum pressure from 57.8 (IQR: 54.3 to 60.3) mm Hg to 73.7 (IQR: 69.5 to 80.8) mm Hg ($p < 0.001$) (Figure 6A), reduced the median LVEDP from 18.8 (IQR: 13.3 to 21.9) mm Hg to 17.8 (IQR: 9.9 to 20.4) mm Hg ($p < 0.001$), and reduced the median left atrial pressure from 15.6 (IQR: 12.9 to 19.3) mm Hg to 12.4 (IQR: 8.9 to 16.5) mm Hg ($p < 0.001$) (Figures 6B and 6D). In addition, the median ejected stroke volume per heartbeat increased from 35 (IQR: 18.2 to 50.5) ml to 52.6 (IQR: 49.4 to 63.6) ml ($p < 0.001$) (Figure 6C). Device support for 30 min carried on the improvement of LV maximum pressure at 72.3 (IQR: 70.4 to 75.4) mm Hg ($p = 0.196$) mm Hg, LVEDP at 17.4 (IQR: 9.2 to 19.7) mm Hg ($p > 0.999$), left atrial pressure at 12.6 (IQR: 9.6 to 14.5) mm Hg ($p = 0.169$) and stroke volume at 56.7 (IQR: 51.1 to 69.9) ml ($p > 0.999$) (Figure 6, Video 2).

IMPROVEMENT OF HEMODYNAMICS. We demonstrated significant improvement in hemodynamic parameters: the median mean arterial pressure reached 49.40 (IQR: 43.90 to 54.90) mm Hg after 5 min from 40.50 (IQR: 39.20 to 42.10) mm Hg at LVSD status ($p < 0.001$), which preserved over 30 min at 49.1 (IQR: 43.2 to 52.5) mm Hg (Figure 7A). Median aortic blood flow increased from 1.6 (IQR: 1.3 to 1.9) l/min to 2.1 (IQR: 1.9 to 2.6) l/min ($p < 0.001$) after 5 min without significant change after 30 min of device actuation; 2.2 (IQR: 1.7 to 2.3) l/min ($p > 0.999$)

FIGURE 3 Mechanical Effect of Soft Robotic Ventricular Assist Device With Septal Bracing on LV Geometry

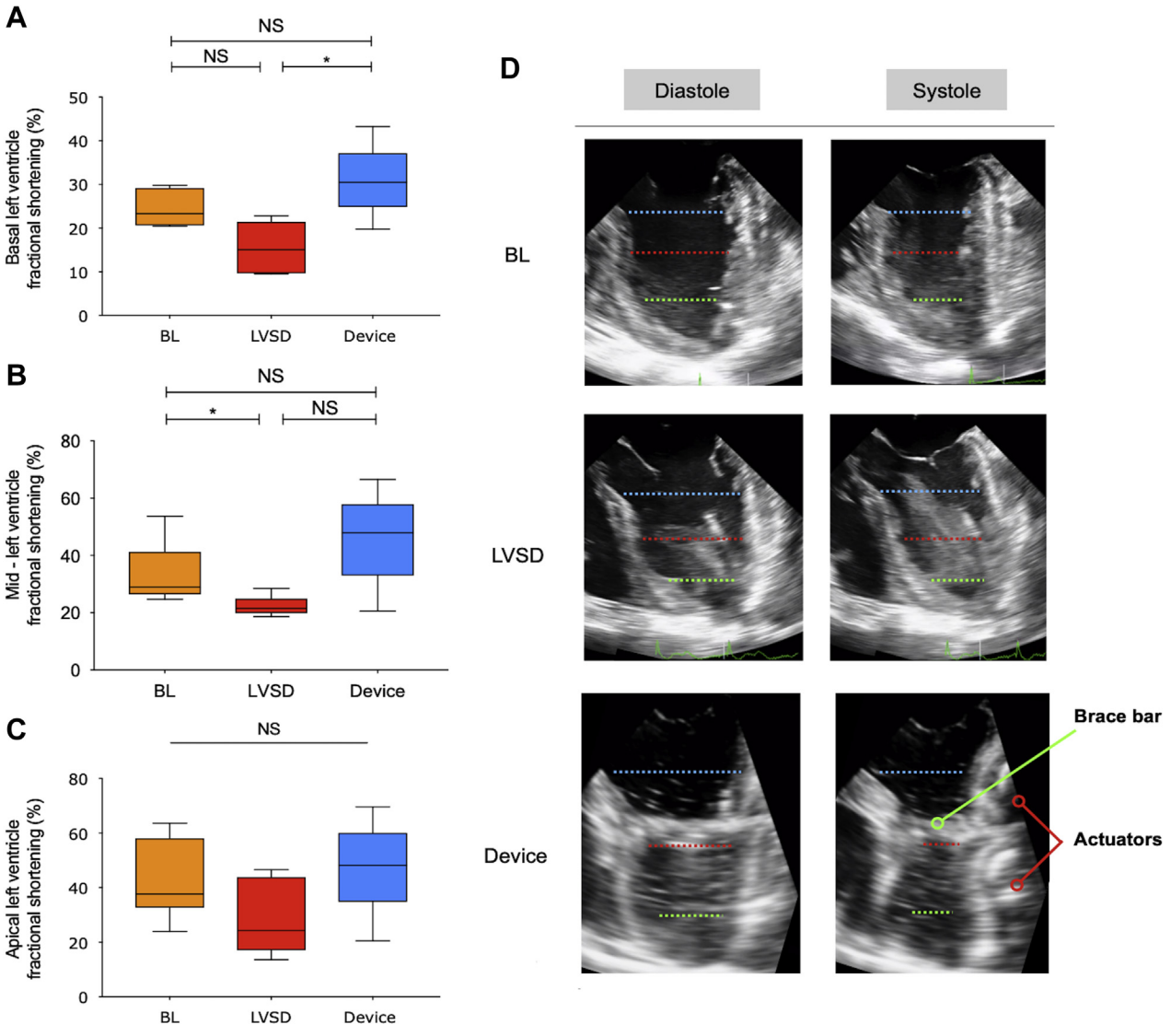

Fractional shortening (FS) proportion of the left ventricle (LV) at **(A)** the LV basal level, **(B)** the mid-LV level, and **(C)** the LV apex. Level of FS measurement are marked with **dashed lines**: LV basal level with **blue**, the mid-LV level with **red**, and LV apex with **green**. **(D)** Echocardiographic view of the LV showing the distance changes between the LV free wall and the interventricular septum (IVS) at normal baseline (BL), induction of LV systolic dysfunction (LVSD), and during device actuation. *p = 0.031. NS = not significant.

(Figure 7B). In addition, reducing the left atrial end-diastolic pressure and LVEDP led to improvement in pulmonary blood flow from 2.1 (IQR: 1.9 to 2.5) l/min to a median of 2.4 (IQR: 2.4 to 2.8) l/min at 5 min ($p < 0.001$) and 2.4 (IQR: 2.1 to 2.7) l/min at 30 min (Figure 7C).

PROVISION OF PULSATILE FLOW. Synchronized augmentation of the LV affects the natural pulsatile flow (Figure 7D), which is essential for maintaining myocardial and heart valve function, as well as arterial wall thickness (27-29). To evaluate flow pulsatility, we compared the pulse pressure (the difference between the maximum and minimum pressure in the pulse wave) and the surplus hemodynamic energy, a metric that quantifies variations in pulsatile energy in pressure and flow waveforms (30,31). After 5 min of device operation, the median pulse pressure returned to the baseline level (27.2 [IQR: 25.1 to 29.2] mm Hg at baseline vs. 27.1 [IQR: 24.8 to 29.6] mm Hg during SRVAD operation; $p > 0.999$), with a significant improvement

FIGURE 4 Soft Robotic Device Effect on Mitral Valve Geometry

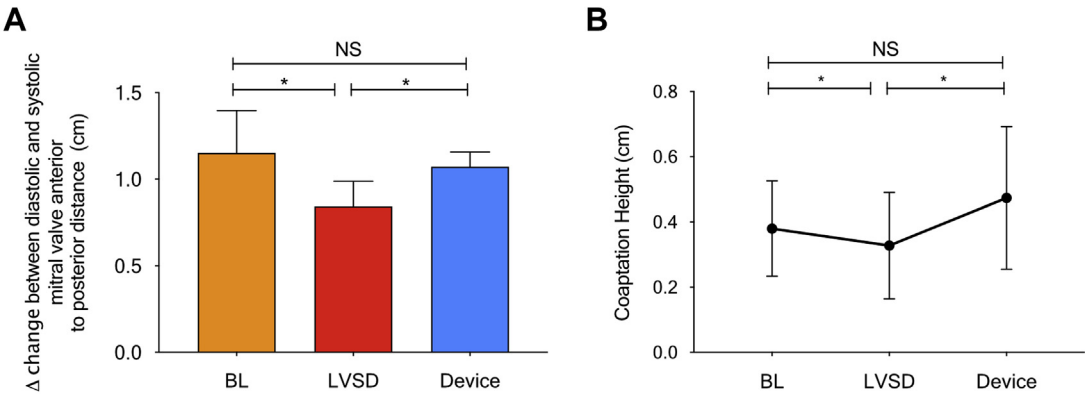

(A) Delta change among the anterior to posterior points of the mitral valve annulus at end-diastole and end-systole at BL, after induction of LVSD, and after device actuation. **(B)** Change in mitral valve coaptation height at BL, after induction of LVSD, and after device actuation. *p = 0.031. Abbreviations as in Figure 3.

FIGURE 5 Soft Robotic Device Effect on Mitral Valve Function

A

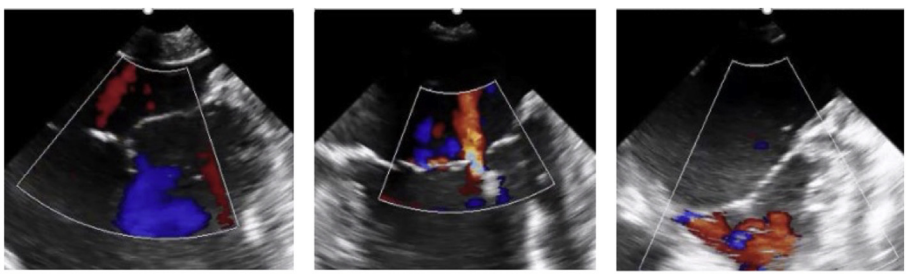

B

	Baseline	LVSD	Device	*P* value
MVR	No	Mild	No	0.125
Vena contracta (cm)	0	0.35 ± 0.9	0	0.125

(A) Two-dimensional color Doppler echocardiographic images showing mitral valve regurgitation (MVR) changes at baseline, after induction of left ventricular systolic dysfunction (LVSD), and after device actuation. **(B)** MVR grade and vena contracta diameter at baseline, after induction of LVSD, and after device actuation. See Video 1.

FIGURE 6 Left Ventricular Hemodynamic Changes After Applying Soft Robotic Device

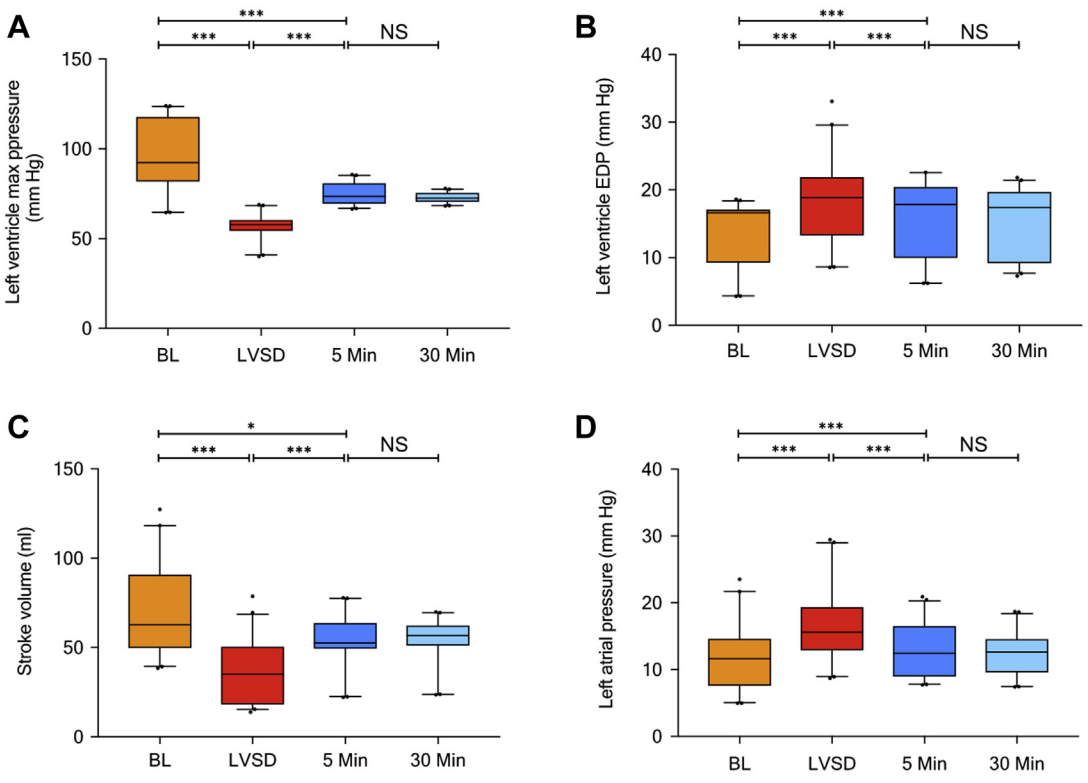

Boxplots of **(A)** LV maximum pressure, **(B)** LV end-diastolic pressure (EDP), **(C)** stroke volume, and **(D)** left atrial pressure at baseline (BL), after induction of LVSD, and after continuous device actuation for 5 and 30 min. See Video 2. *p = 0.024, ***p < 0.001. Abbreviations as in Figure 3.

from induction of LVSD (22.1 [IQR: 19.7 to 23.2] mm Hg; p < 0.001) (Figure 8A). Surplus hemodynamic energy increased to 14.5 ± 4.0 × 10^3 erg/cm^3 in 5 min and 15.4 ± 3.6 × 10^3 erg/cm^3 after 30 min of SRVAD operation (12.8 ± 3.3 × 10^3 erg/cm^3 at baseline; p = 0.182) from 10.5 ± 2.1 × 10^3 erg/cm^3 at LVSD status (p = 0.007) (Figure 8B). These effects in surplus hemodynamic energy were maintained for 30 min of device actuation (p = 0.126).

ACUTE LVSD MODEL. Using our short-term method to create LVSD, as described in detail in the Methods, we induced a significant reduction in LV function, shown as a reduction in LV ejection fraction from 51.9 ± 7.6% at baseline to 40.5 ± 7.2% (p = 0.002), a reduction in stroke volume from a median of 62.9 (IQR: 49.6 to 90.8) ml to 35.0 (IQR: 18.2 to 50.4) ml (p < 0.001) (Figure 6B), and an increase in LVEDP from a median of 16.6 (IQR: 9.2 to 17.1) mm Hg to 18.8 (IQR: 13.3 to 21.9) mm Hg (p < 0.001) (Figure 6C). The LVSD that was generated led to a significant drop in mean arterial pressure by 46.8%, from a median of 76.00 (IQR: 74.20 to 92.40) mm Hg to 40.47 (IQR: 39.20 to 42.10) mm Hg (p < 0.001) (Figure 7A), and aortic blood flow by 50.6%, from 3.4 (IQR: 2.9 to 3.7) l/min to 1.7 (IQR: 1.3 to 1.9) l/min (p < 0.001) (Figure 7B).

DISCUSSION

In this work, SRVAD actuation significantly reduced the MV anterior-to-posterior distance during systole at MV annulus level and submitral apparatus, which led to improved valve leaflet coaptation and eliminated MVR.

The device was able to significantly improve motion between the LV free wall and the IVS along the area of application, especially at the LV basal level, generating marked improvement in LV pressure during LV systole compared with that in the LVSD

FIGURE 7 Effect of Soft Robotic Device on Hemodynamics

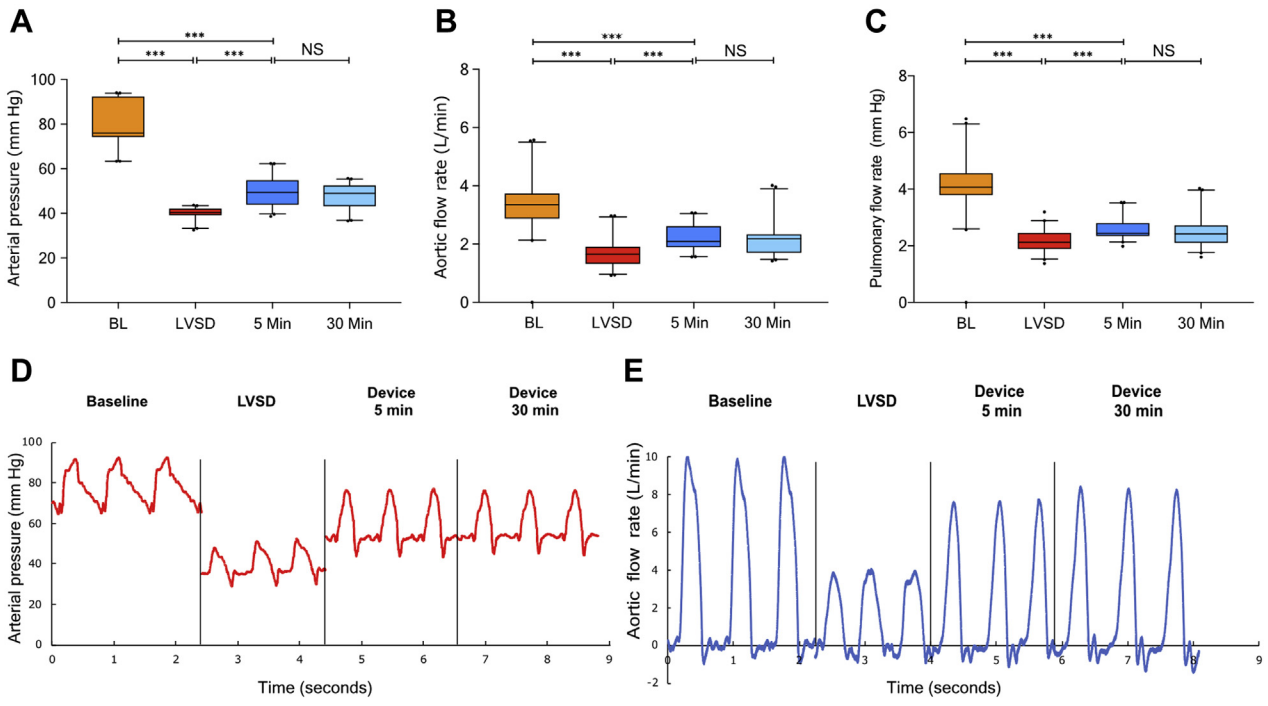

Boxplots of **(A)** mean arterial pressure, **(B)** aortic flow rate, and **(C)** pulmonary flow rate at BL, after induction of LVSD, and after continuous device actuation for 5 and 30 min. **(D, E)** Plots showing aortic pressure versus time and aortic flow rate at BL, after induction of LVSD, and with the device actuated at 5 and 30 min. ***$p < 0.001$. Abbreviations as in Figure 3.

condition. In addition, the device aided relaxation of the LV during diastole, improving the LV filling pressure, as shown by the alleviation of LVEDP and left atrial pressure. Reduction of LVEDP and left atrial pressure is critical for preventing the progression of right-side HF (cor pulmonale), as was evident from the reduction in pulmonary blood flow with LVSD, which improved significantly during SRVAD operation.

Furthermore, the device's effect on LV noticeably improved systemic arterial pressure and arterial flow with a pulsatile wave comparable to natural pulsation.

The implementation of soft robotics in cardiac support allows a low risk of harming myocardial tissues and the ability to adjust the actuator shape to natural ventricular wall structure (32). Direct augmentation of a native ventricular myocardium and enhancement of the ventricular wall mobility through SRVAD actuation may prevent deterioration of myocardial function. Previously, our group has demonstrated promising results of isolated LV and RV support using soft robotic devices in Short-term animal models (23,33). Previous work on the use of external sleeves and soft robotic devices showed promising improvement in ventricular function and hemodynamic support; the devices were designed to apply direct cardiac compressions to the ventricles and support heart with severe biventricular dysfunction (23,34-36). In contrast, interventricular septal anchoring provided the SRVAD with the flexibility to be applied to 1 target ventricle. Moreover, septal anchoring allows control of the position of the IVS and prevents the septal shift that may occur with progressive deterioration of LV function, affecting RV function (37). Synchronized actuation with native myocardial mechanical activity allows the device to assist with LV filling and would allow improving the IVS desynchrony (38-40). Reducing left atrial pressure and LVEDP and improving pulmonary blood flow may also reduce the risk of developing RV function deterioration, which usually follows LV dysfunction (41,42).

FIGURE 8 Soft Robotic Device Provides Pulsatile Flow

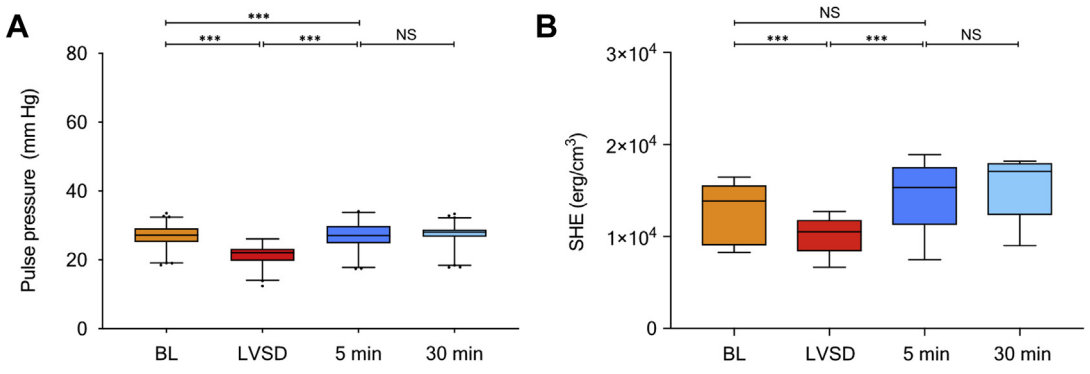

(A) Boxplots of pulse pressure at BL, after induction of LVSD, and after continuous device actuation for 5 and 30 min. **(B)** Boxplots of surplus hemodynamic energy (SHE), which represents the change in pulsatility, at BL, after induction of LVSD, and with the device actuated at 5 and 30 min. *p = 0.028, **p = 0.007, ***p < 0.001. Abbreviations as in Figure 3.

The design of the SRVAD device features a small footprint of the intracardiac components, which minimizes direct blood contact and reduces the need for aggressive systemic anticoagulation, and potentially lowers the risk of clot formation or bleeding events (43,44). The performance of the SRVAD demonstrates its capability of maintaining pulsatile flow with ventricular augmentation in a short testing period. Recent clinical studies elaborate the disadvantage of loss of pulsatile flow, as it increases the incidence of aortic valve regurgitation, reduces arterial wall thickness, and increases sympathetic tone (28,45,46). The nonpulsatile nature of current continuous-flow ventricular assist devices results in the degradation of von Willebrand factor, which is linked to serious complications such as gastrointestinal bleeding (47).

A significant advantage of the SRVAD is the potential of using it for high-risk patients, who, from an intervention perspective, are treated solely for MVR without feasibility for simultaneous intervention to improve LV dysfunction. Most patients with LVSD with associated MVR are considered to be at high risk for surgical intervention on the LV and therefore do not receive an operation (48). Current approaches attempt to improve MV function by using interventional procedures solely aimed at either the MV leaflets (MitraClip) or the annulus (Carillon or Cardioband [Edwards Lifesciences, Irvine, California]) (20). However, such solutions take the LV out of the equation and rely only on MV repair to improve ventricular function. Separate efforts were directed at restoring LV geometry with only passive devices. The CorCap system (Acorn Cardiovascular, St. Paul, Minnesota) aimed to improve LV function but led to an increase in the LV filling pressures and failed to provide significant benefit for the MV (49,50). The Coapsys device, on the other hand, improved the MVR but did not provide significant support for the LV (21). In contrast, the SRVAD provides dynamic changes in LV geometry and without restricting the LV filling, and—importantly—allows simultaneous support at both the MV annulus and the LV basal levels, which helps to improve LV and MV dysfunction combined.

STUDY LIMITATIONS. A short-term study limited our ability to evaluate the mechanical effect of the SRVAD on myocardial tissue and potential reverse remodeling of the myocardium. Evaluation of other biomedical markers for LV dysfunction and systemic effects, including renal function and peripheral tissue perfusion, is not achievable with a short-term model. Furthermore, our acute LVSD model does not completely reflect a typical representation of chronic onset of LV dysfunction and more severe changes in LV geometry. We believe that the limited LV geometric changes led to a lesser grade of MVR at LVSD. Additional mid- and long-term studies with comprehensive assessment of LV mechanics are necessary to determine how this device will impact myocardial function.

In upcoming work, we are planning to test device performance in a chronic LVSD swine model by

inducing ischemic cardiomyopathy with controlled microembolization in the left coronary arteries. The chronic model will produce severe geometric changes in the LV with an advanced MVR. We are planning to develop a next generation of a miniaturized SRVAD that would be deployed through a mini-thoracotomy incision. Moreover, we are attempting to add strain and pressure sensors to the extracardiac and the intracardiac components of the device respectfully to real-time monitor LV response to the SRVAD augmentation and incorporate the signal into a closed-loop control system. Furthermore, comprehensive histological and tissue response characterization will be incorporated into the future, mid- and long-term studies.

In addition, we will perform a more focused evaluation on the right ventricle and tricuspid valve functions. As we observed worsening of tricuspid valve regurgitation when the septal anchor is closed to the septal leaflet chordae of tricuspid valve (Supplemental Figure 1). On the opposite, when the anchor is away from septal leaflets and chordae, the tricuspid function did not change with device actuation. (Supplemental Figures 2 and 3)

ACKNOWLEDGMENTS The authors would like to thank Dr. A. Nedder, N. Crilley, E. Pollock, C. Pimental and M. Woomer from Animal Research Children's Hospital team for their help facilitating animal experiments.

ADDRESS FOR CORRESPONDENCE: Dr. Nikolay V. Vasilyev, Department of Cardiac Surgery, Boston Children's Hospital, Harvard Medical School, 300 Longwood Avenue, Boston, Massachusetts 02115. E-mail: nikolay.v.vasilyev.md@gmail.com.

PERSPECTIVES

COMPETENCY IN MEDICAL KNOWLEDGE: Implantable soft robotic devices are uniquely capable of augmenting the native tissue shape and function, which generates growing interest in use of soft robotics in clinical practice. In this study, we were able to use these unique abilities of a SRVAD to dynamically augment native LV and MV functions in synchrony.

TRANSLATIONAL OUTLOOK: Future device design improvements will focus on the incorporation of integrated hemodynamic pressure-sensing systems and electrogram sensors integrated into the brace bar. Furthermore, a compact and portable control system will be needed for chronic studies and clinical translation. With respect to the procedural enhancements, simplification of the deployment process to 1 or 2 steps will allow the device to be implanted rapidly in a minimally invasive procedure. We anticipate testing the device in a chronic animal model of HF, with survival for up to 8 to 12 weeks. Taking these steps forward will facilitate translation of this technology to clinical practice.

REFERENCES

1. Benjamin EJ, Blaha MJ, Chiuve SE, et al. Heart Disease and Stroke Statistics—2017 Update: a report from the American Heart Association. Circulation 2017;135:e146–603.

2. Lloyd-Jones DM, Larson MG, Leip EP, et al. Lifetime risk for developing congestive heart failure: the Framingham Heart Study. Circulation 2002;106:3068–72.

3. Vasan RS, Xanthakis V, Lyass A, et al. Epidemiology of left ventricular systolic dysfunction and heart failure in the Framingham Study. J Am Coll Cardiol Img 2018;11:1–11.

4. Yancy CW, Jessup M, Bozkurt B, et al. 2017 ACC/AHA/HFSA Focused Update of the 2013 ACCF/AHA Guideline for the Management of Heart Failure. J Am Coll Cardiol 2017;70:776–803.

5. Nishimura RA, Otto CM, Bonow RO, et al. 2017 AHA/ACC Focused Update of the 2014 AHA/ACC Guideline for the Management of Patients With Valvular Heart Disease: a report of the American College of Cardiology/American Heart Association Task Force on Clinical Practice Guidelines. J Am Coll Cardiol 2017;70:252–89.

6. Yeboah J, Rodriguez CJ, Stacey B, et al. Prognosis of individuals with asymptomatic left ventricular systolic dysfunction in the Multi-Ethnic Study of Atherosclerosis (MESA). Circulation 2012;126:2713–9.

7. Mozaffarian D, Benjamin EJ, Go AS, et al. Heart Disease and Stroke Statistics—2016 Update. Circulation 2016;133:e38–360.

8. Kaplan SR, Bashein G, Sheehan FH, et al. Three-dimensional echocardiographic assessment of annular shape changes in the normal and regurgitant mitral valve. Am Heart J 2000;139:378–87.

9. McCarthy KP, Ring L, Rana BS. Anatomy of the mitral valve: understanding the mitral valve complex in mitral regurgitation. Eur J Echocardiogr 2010;11:i3–9.

10. Asgar AW, Mack MJ, Stone GW. Secondary mitral regurgitation in heart failure. J Am Coll Cardiol 2015;65:1231–48.

11. Ennezat PV, Maréchaux S, Pibarot P, Le Jemtel TH. Secondary mitral regurgitation in heart failure with reduced or preserved left ventricular ejection fraction. Cardiology 2013;125:110–7.

12. Samad Z, Shaw LK, Phelan M, et al. Management and outcomes in patients with moderate or severe functional mitral regurgitation and severe left ventricular dysfunction. Eur Heart J 2015;36:2733–41.

13. Mowakeaa S, Dwivedi A, Grossman JR, et al. Prognosis of patients with secondary mitral regurgitation and reduced ejection fraction. Open Heart 2018;5:e000745.

14. Gaasch WH, Meyer TE. Left ventricular response to mitral regurgitation. Circulation 2008;118:2298–303.

15. Dogan G, Hanke JS, Ricklefs M, et al. MitraClip procedure prior to left ventricular assist device implantation. J Thorac Dis 2018;10 Suppl 15:S1763–8.

16. Arsalan M, Squiers JJ, DiMaio JM, Mack MJ. Catheter-based or surgical repair of the highest risk secondary mitral regurgitation patients. Ann Cardiothorac Surg 2015;4:278–83.

17. Maisano F, Torracca L, Oppizzi M, et al. The edge-to-edge technique: a simplified method to correct mitral insufficiency. Eur J Cardiothoracic Surg 1998;13:240–6.

18. Vakil K, Roukoz H, Sarraf M, et al. Safety and efficacy of the MitraClip ® system for severe mitral regurgitation. Catheter Cardiovasc Interv 2014;84:129–36.

19. Schäfer U, Deuschl F, Schofer N, Lubos E, Blankenberg S. Critical evaluation of the MitraClip

system in the management of mitral regurgitation. Vasc Health Risk Manag 2016;12:1–8.

20. Lipiecki J, Siminiak T, Sievert H, et al. Coronary sinus-based percutaneous annuloplasty as treatment for functional mitral regurgitation: the TITAN II trial. Open Heart 2016;3:e000411.

21. Grossi EA, Patel N, Woo YJ, et al. Outcomes of the RESTOR-MV Trial (Randomized Evaluation of a Surgical Treatment for Off-Pump Repair of the Mitral Valve). J Am Coll Cardiol 2010;56:1984–93.

22. Han JJ, Acker MA, Atluri P. Left ventricular assist devices. Circulation 2018;138:2841–51.

23. Payne CJ, Wamala I, Bautista-Salinas D, et al. Soft robotic ventricular assist device with septal bracing for therapy of heart failure. Sci Robot 2017;2:eaan6736.

24. Payne CJ, Wamala I, Abah C, et al. An implantable extracardiac soft robotic device for the failing heart: mechanical coupling and synchronization. Soft Robot 2017;4:241–50.

25. Sabbah HN, Stein PD, Kono T, et al. A canine model of chronic heart failure produced by multiple sequential coronary microembolizations. Am J Physiol 1991;260:H1379–84.

26. Monreal G, Sherwood LC, Sobieski MA, Giridharan GA, Slaughter MS, Koenig SC. Large animal models for left ventricular assist device research and development. ASAIO J 2014;60:2–8.

27. Kato TS, Chokshi A, Singh P, et al. Effects of continuous-flow versus pulsatile-flow left ventricular assist devices on myocardial unloading and remodeling. Circ Heart Fail 2011;4:546–53.

28. Barić D. Why pulsatility still matters: a review of current knowledge. Croat Med J 2014;55:609–20.

29. Bartoli CR, Giridharan GA, Litwak KN, et al. Hemodynamic responses to continuous versus pulsatile mechanical unloading of the failing left ventricle. ASAIO J 2010;56:410–6.

30. Shepard RB. Energy equivalent pressure. Arch Surg 1966;93:730–40.

31. Soucy KG, Koenig SC, Giridharan GA, Sobieski MA, Slaughter MS. Defining pulsatility during continuous-flow ventricular assist device support. J Heart Lung Transplant 2013;32:581–7.

32. Wamala I, Roche ET, Pigula FA. The use of soft robotics in cardiovascular therapy. Expert Rev Cardiovasc Ther 2017;15:767–74.

33. Horvath MA, Wamala I, Rytkin E, et al. An intracardiac soft robotic device for augmentation of blood ejection from the failing right ventricle. Ann Biomed Eng 2017;45:2222–33.

34. Anstadt MP, Budharaju S, Darner RJ, et al. Ventricular actuation improves systolic and diastolic myocardial function in the small failing heart. Ann Thorac Surg 2009;88. 1982–8; discussion 1988.

35. Roche ET, Horvath MA, Wamala I, et al. Soft robotic sleeve supports heart function. Sci Transl Med 2017;9:eaaf3925.

36. Hord EC, Bolch CM, Tuzun E, Cohn WE, Leschinsky B, Criscione JC. Evaluation of the CorInnova Heart Assist Device in an acute heart failure model. J Cardiovasc Transl Res 2019;12:155–63.

37. Klima UP, Lee M-Y, Guerrero JL, LaRaia PJ, Levine RA, Vlahakes GJ. Determinants of maximal right ventricular function: role of septal shift. J Thorac Cardiovasc Surg 2002;123:72–80.

38. Breithardt OA, Claus P, Sutherland GR. Do we understand who benefits from resynchronisation therapy? Eur Heart J 2004;25:535–6.

39. Bleeker GB, Schalij MJ, Molhoek SG, et al. Frequency of left ventricular dyssynchrony in patients with heart failure and a narrow QRS complex. Am J Cardiol 2005;95:140–2.

40. Ghio S, Constantin C, Klersy C, et al. Interventricular and intraventricular dyssynchrony are common in heart failure patients, regardless of QRS duration. Eur Heart J 2004;25:571–8.

41. Argiriou M, Kolokotron S-M, Sakellaridis T, et al. Right heart failure post left ventricular assist device implantation. J Thorac Dis 2014;6 Suppl 1:S52–9.

42. Meineri M, Van Rensburg AE, Vegas A. Right ventricular failure after LVAD implantation: prevention and treatment. Best Pract Res Clin Anaesthesiol 2012;26:217–29.

43. Boyle AJ, Jorde UP, Sun B, et al. Pre-operative risk factors of bleeding and stroke during left ventricular assist device support: an analysis of more than 900 HeartMate II outpatients. J Am Coll Cardiol 2014;63:880–8.

44. Shah N, Agarwal V, Patel N, et al. National trends in utilization, mortality, complications, and cost of care after left ventricular assist device implantation from 2005 to 2011. Ann Thorac Surg 2016;101:1477–84.

45. Takeda K, Takayama H, Kalesan B, et al. Long-term outcome of patients on continuous-flow left ventricular assist device support. J Thorac Cardiovasc Surg 2014;148:1606–14.

46. Bozkurt S. Arterial pulsatility and aortic valve function under continuous flow left ventricular assist device support, continuous speed vs. varying speed pump assistance (PhD thesis). Eindhoven: Technische Universiteit Eindhoven, 2014. 127 p. Available at: https://doi.org/10.6100/IR777492. Accessed February 9, 2020.

47. Bartoli CR, Zhang DM, Hennessy-Strahs S, et al. Clinical and in vitro evidence that left ventricular assist device-induced von Willebrand factor degradation alters angiogenesis. Circ Heart Fail 2018;11:e004638.

48. Nappi F, Avatar Singh SS, Santana O, Mihos CG. Functional mitral regurgitation: an overview for surgical management framework. J Thorac Dis 2018;10:4540–55.

49. Acker MA, Bolling S, Shemin R, et al. Mitral valve surgery in heart failure: Insights from the Acorn Clinical Trial. J Thorac Cardiovasc Surg 2006;132:568–77.e4.

50. Acker MA, Jessup M, Bolling SF, et al. Mitral valve repair in heart failure: Five-year follow-up from the mitral valve replacement stratum of the Acorn randomized trial. J Thorac Cardiovasc Surg 2011;142:569–74.e1.

KEY WORDS left ventricular systolic dysfunction, mitral valve, secondary mitral regurgitation, soft robotic

APPENDIX For supplemental figures and videos, please see the online version of this paper.